

A lightweight slotted elliptical patch with defected ground printed monopole antenna for microwave based biomedical imaging applications

MD SIAM TALUKDER¹, MOHAMMAD TARIQUL ISLAM², NEBRAS SOBAHI³, MD. MONIRUZZAMAN², MD. MOTTAHIR ALAM³, TANVEER AHSAN⁴, MD SAMSUZZAMAN^{1,5,*}

¹*Dept. of Computer and Communication Engineering, Faculty of Computer Science and Engineering, Patuakhali Science and Technology University, Patuakhali, Bangladesh*

²*Dept of Electrical, Electronic and Systems Engineering, Universiti Kebangsaan Malaysia Selangor, Malaysia*

³*Department of Electrical and Computer Engineering, King Abdulaziz University, Jeddah 21589, Saudi Arabia*

⁴*Department of Computer Science and Engineering, International Islamic University Chittagong (IIUC), Bangladesh*

⁵*Department of General Educational Development (GED), Faculty of Science and Information Technology (FSIT), Daffodil International University, Bangladesh*

This article describes the design of a new Slotted Elliptical Patch with Defected Ground Antenna (SEPDGA) for microwave-based imaging applications. The intended antenna comprises of a defective ground plane and multiple rectangular slotted ellipse-shaped patch. Multi-resonances can be exhibited by the designed antenna which merges to disclose the wideband spectrum. The experimentally verified antenna has a fractional bandwidth (FBW) of 79% and a functional frequency band of 1.3–3.0 GHz (< -10 dB). According to simulation-based outcomes, it operates between 1.4 -3.2 GHz and has an FBW of 78%. Additionally, the antenna prototype has achieved a highest gain of 4.9 dBi at 2.65 GHz and an efficiency peak of above 85%. In addition to demonstrating superior time domain behaviors as well as omnidirectional radiation properties across the entire operating spectrum. Featuring a compact size, decent gain, high fidelity, large band of operation and efficiency, as well as stable omnidirectional radiation characteristics, this antenna is perfect for applications in biomedical imaging.

(Received March 8, 2022; accepted October 5, 2022)

Keywords: Slotted Elliptical Patch, Defected Ground Antenna, Microwave-Based Imaging Applications

1. Introduction

Antennas are commonly used as basic equipment in wireless applications as they're front-end devices [1, 2]. It is necessary for the transmission and reception of electromagnetic waves in empty space. Contemporary communications demonstrate that antennas could also be used for a variety of purposes, such as transportable wireless devices [3, 4], military applications [5], radar applications [6], biological imaging applications [7, 8], and so on. A wide variety of biomedical applications have used antennas in recent years, either transplanted in the body organ or externally placed as in biomedical imaging [9]. EMI (Electromagnetic Imaging) in Microwave and Millimeter-wave frequency ranges is a promising replacement for expensive diagnostic devices for medical imaging owing to the concern about human health, as well as the ability to use antennas. A fundamental element of EMI is the transmission of an electromagnetic (EM) wave from one antenna to another which travels through the targeted medium and is received by the receiving antenna (for bistatic) or multiple antennas (for multistatic) on a

different side of the medium. A variation in the wave response happens whenever the traveling signal travels into an organ with differing dielectric characteristics. An instance of this occurs in biological objects when the dielectric properties of tissues discontinue. A receiving antenna or an array of antennas collects backscattered waves after incident waves scatter back. Thus, the biomedical EMI is based on the observation of the signal responses of the received signals caused by differing dielectric characteristics between healthy and abnormal malignant tissue.

Microwave Imaging (MWI) for biomedical imaging areas uses non-ionizing radiation as opposed to conventional brain MRIs or brain CTs, which are problematic for claustrophobic patients and they need the use of ionizing radiation. MWI as well needs fewer equipment than another two traditional methods (MRIs and CTs). MWI is generally safe, affordable, and inexpensive, particularly for the cheap transmitter and the receiver. Researchers have presented several research articles about microwave imaging for brain tumor detection in [10-13]. In [13], a stroke imaging technique

using microwaves with antipodal Vivaldi antenna ($50 \times 60 \text{ mm}^2$) is developed and discussed. An array with 9 antipodal Vivaldi antenna element with frequencies ranging from 2.06 - 2.61 GHz were reported throughout this work. As shown in [14], the antenna is designed as a dipole with multiple slots and four shorting pins that operate at different frequencies. The imaging system incorporates a flexible dielectric substrate that has a high permittivity, resulting in a small sensor antenna. As the antenna is small ($25 \times 28 \text{ mm}^2$), but have less bandwidth, the deep-lying malignancy are tricky to diagnose. In [15], an EBG based and metamaterial-based antenna is reported. The planned antenna comprises of a 4×4 radiating element filled with symmetrically elongated U-slots being fed by a combo of serial and parallel transmission line. Antenna bandwidth: 53.8% (1.16-1.94 GHz), a radiation effectiveness of about 80%, but gain flatness is not evident throughout the spectrum. A number of other antennas are also being proposed by researchers at MWI, including directional/omnidirectional printed patch antennas [16-19] CPW fed antennas, 3-D antennas, and Vivaldi antennas [20-22].

In this research work, a lightweight Slotted Elliptical Patch with Defected Ground (SEPDGA) printed monopole antenna for microwave based biomedical imaging purposes is described. This antenna prototype functions between 1.3 – 3.0 GHz (experimental) and is fabricated on 1.5 mm thin FR-4 substrates. The substrate has a relative permittivity of 4.3 and a loss tangent of 0.0027, respectively. The antenna dimensions were tuned to be $57 \times 38 \times 1.6 \text{ mm}^3$ and electrically to be $0.26 \times 0.17 \times 0.007 \lambda^3$ (λ is the wavelength of 1.4 GHz). The presented work is innovative due to its small size and increased bandwidth, as well as its additional features and functionalities that may mitigate the shortcomings of existing antennas, such as their low gain, limited bandwidth, and non - implementation with realistic head models. The antenna decreases its dimensions by 26% compared to comparable contemporary antennas, increases its FBW, gives adequate gain, and has improved radiation characteristics. Because of its inherent simplicity and small size, the antenna may be easily integrated into a wide variety of miniature biological applications. Antenna placement is flexible since the antenna has a stable-omnidirectional radiation properties and can be placed in front or behind the human head.

2. SEPDGA-design evolution, optimization and final layout

Starting with a conventional monopole Elliptical Patch Antenna (EPA), the proposed antenna is designed as shown in phase 1: Fig. 1. EPAs primarily offer wideband properties on FR-4 substrates; however, these basic layouts have limits in terms of enhancing optimum

performance of the antenna. As a result, those traditional forms are modified in this work using a hierarchical design approach. By focusing on its various benefits, the substrate material used here is FR4 substrate with a permittivity of 4.3. Generally, substrates made of FR4 epoxy are widely used in printed circuit board production. Because of its cheap price and high mechanical qualities, the material is highly desirable for use in a variety of electronic component designs. Significant effort is being put into reducing the price of microwave systems as they are increasingly developed for growth markets. It is possible to obtain significant cost reductions by using FR4 as the substrate for microwave antennas rather than the more expensive PTFE-based options. In addition to being durable and water-resistant, these materials provide superior insulation within copper layers, which reduces interference and helps ensure high-quality signal transmission. The elliptical patch was rectangular slotted in the second phase. The conventional path of the surface current was changed by this slotting method. As a result, the current is dispersed across a vast region. As a result, the higher frequency was moved forward 200 MHz, and the functioning impedance bandwidth (IBW) increased compared to the preceding phase. In the third phase, a rectangular slot is incorporated into the back radiator. This slot also obstructs the usual current path in the back radiator, resulting in more radiation via the back radiator. This additional radiation creates another resonance mode in higher-frequency. However, the computed reflection coefficient results in Fig. 2 reveal that the layout offers multiple notch band about 1.8 GHz and 2.5 GHz, indicating that it does not attain a wide working range. With the previously defective ground plane structure, extra two rectangular slots were added to the patch structure in the proposed phase, which affects surface current more correctly. This phase additionally improves the inductive and capacitive effects, resulting in impedance bandwidth $\leq -10 \text{ dB}$ in a range of 1.4 GHz to 3.2 GHz, thus provides a higher IBW (1.4 GHz to 3.2 GHz) with three resonance points at 1.57 GHz, 2.1 GHz and 2.4 GHz, respectively.

After the evolution of SEPDGA, a parameterized analysis is conducted using CST simulator to examine the influence of different parts on the antenna performance. Changing $C4$, $K3$, $C3$ and $C2$ parameters appears to change antenna properties. Fig. 3(a-d) depicted the simulated reflection coefficient for various $C4$ and $K3$ values. There is a significant mismatch between functional band for values lesser or greater as compared to the optimal value of 32.5 mm for $C4$, which results in a decreased working band. When $C4$ values were reduced below the optimal value, the higher frequency moved 200 MHz backward, resulting in a reduction in bandwidth. Furthermore, the impedance is not effectively matched with the lowered value, resulting in a poor reflection coefficient above-20 dB in higher frequency. Again, with a higher value of $C4$ than the intended value, the antenna exhibits poorer radiation efficiency at around 2.27 GHz. As a result, the impedance band is extremely near to -10 dB at that point. However, as seen in Fig. 3(b), $K3$ of the SEPDGA considerably accentuates antenna impedance

matching. If the value is lowered, the higher frequency moves back 200 MHz, resulting in a lower IBW as well as lower resonance mode disappear. When the parameter was increased while the other parameters remained constant, the actual slot area in back radiator shrank, resulting in a narrower current route within the slot and a larger inductive effect. This is due to the fact that the impedances are not matched in this instance, resulting in poor reflection coefficients at about 2.5 GHz. It can be seen that the effective slot area of the ground plane increases when C3 increases by 1 mm compared to the proposed value with all other parameters remaining unchanged. As a direct consequence of this, the length of the current route inside the slot increases, which, in turn, causes the first and second resonance frequencies to move towards. In addition, because of an improper impedance matching, in this case, the antenna exhibits a bad reflection coefficient level that is above -10 dB at around 2.6 GHz as seen in Fig. 3(c). This causes the third resonance to evaporate within a single band. Similarly, whenever the parameter value C3 is lowered by 1 mm, the current route within the

slot gets shorter and the inductive impact is becoming more pronounced. As a consequence of this, the lower resonance is eliminated, and the top frequency moves approximately 500 MHz to the back, which leads to a decrease in effective bandwidth.

Furthermore, the impact of varying the C2 value on the reflection coefficient is seen in Fig. 3(d). If we reduce C2 by 1 mm, we reduce the effective slot area in the top radiator, hence decreasing the current path via the slot and so reducing the capacitive impact. This has an immediate and significant impact on the second resonant frequency. Similarly, when C2 is extended by 1 mm, the slot region in the patch radiator grows. Additionally, the surface current path increases, which causes the capacitive effects to improve. An operating band that was sufficiently wide and a reflection coefficient that was acceptable enough for head imaging were both given by a proposed tuned value of 3 millimeters.

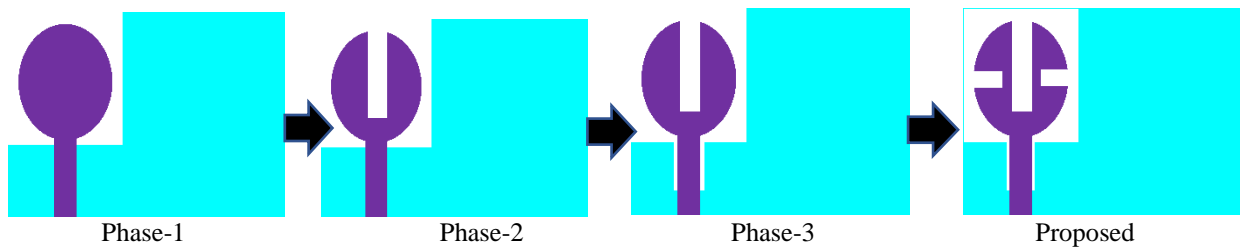


Fig. 1. Different phase of SEP-DGA design evolution (color online)

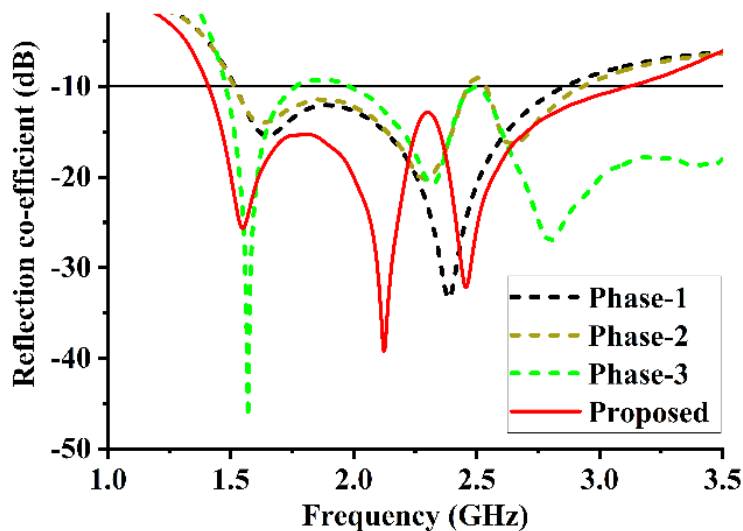


Fig. 2. Simulated reflection coefficient for each step of the evolution phase (color online)

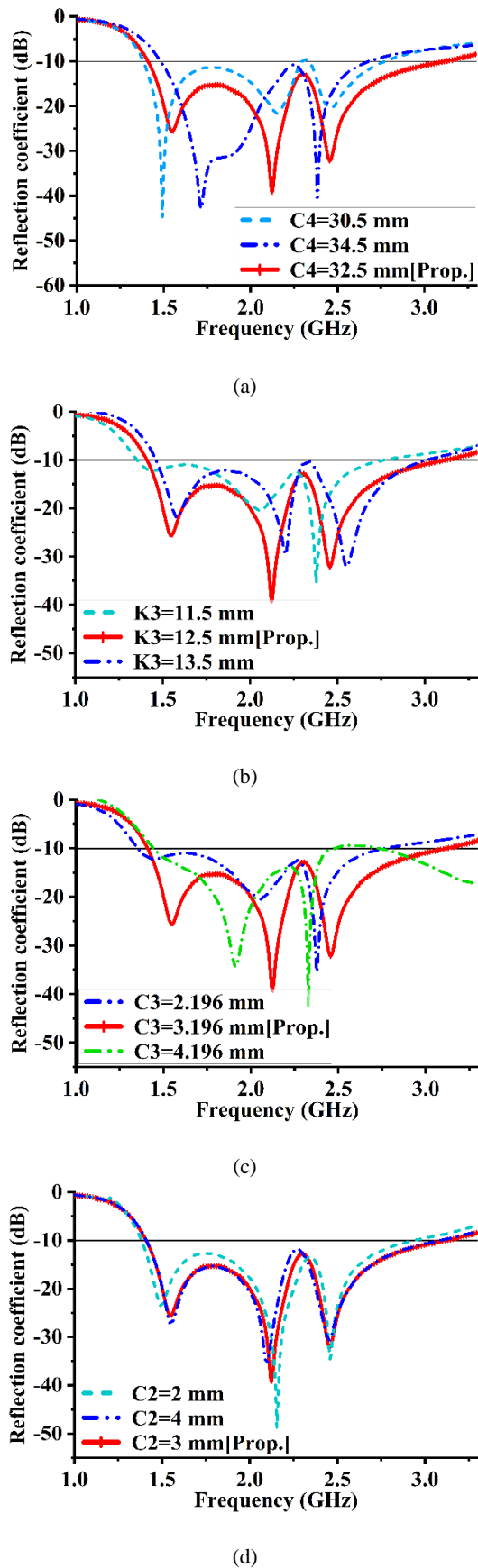


Fig. 3. The influences of changing various parameters on the proposed SEPDGA; (a) $C4$ parameter, (b) $K3$ parameter, (c) $C3$ parameter, (d) $C2$ parameter (color online)

As a final product of SEPDGA evolution and optimization, Fig. 4 depicts the finalized design layout with parametric notation. SEPDGA proposes that front radiator be comprised of three rectangular slots arranged in an elliptical shape, as well as the defected ground structure includes multiple rectangular slots. The antenna is fed by a transmission line with dimensions of $L_f \times W_f \text{ mm}^2$. Here, it's worth noting that the feed line width W_f relates to match the 50Ω impedance. Just below the feed line in the back radiator, a rectangular slot with dimensions of $K4 \times C3 \text{ mm}^2$ was included. Radius V_r represents the major radius, and radius U_r represents the minor radius of the elliptical patch. The ground plane $SL \times SW \text{ mm}^2$ has the same dimensions as the substrate. The antenna is designed and fabricated on a FR-4 substrate material that is both affordable and economical with permittivity of 4.3, dielectric tangent-loss of 0.0037, and thicknesses (h) of 1.5 mm. Table 1 contains the optimal values for all of the parameters related with the final design layout.

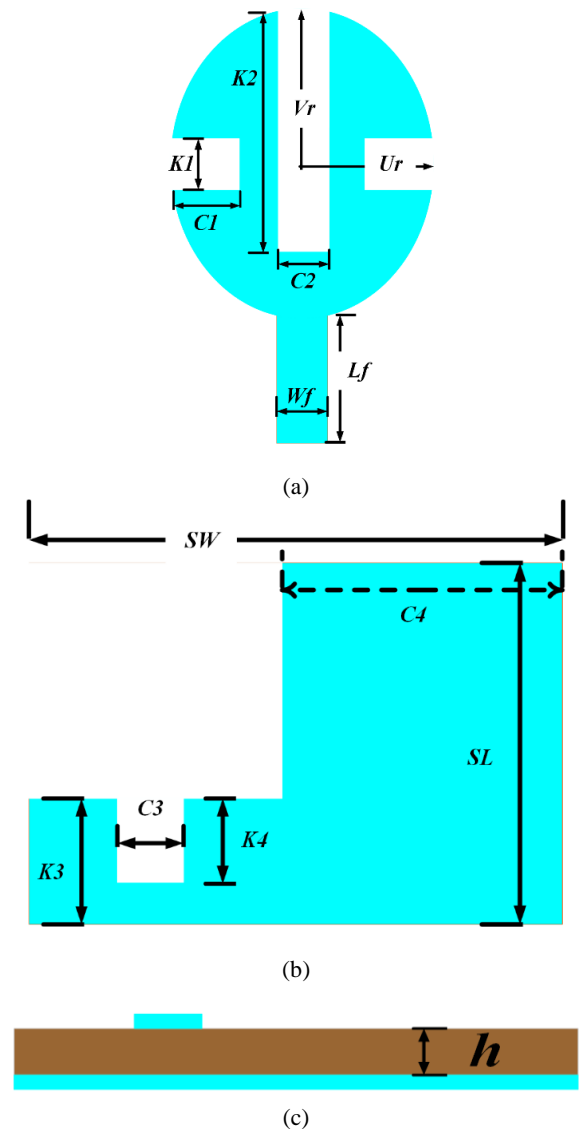


Fig. 4. Optimum layout of the proposed SEPDGA antenna; (a) Patch radiator, (b) Back radiator, (c) Side-view (color online)

Table 1. Design parameters for antennas with optimum values

Parameters	SW	C1	C2	C3	C4	K1	K2
Values (mm)	37	6.83	3	3.196	32.50	4	17.27
Parameters	SL	K3	K4	Vr	Ur	Wf	Lf
Values (mm)	56	12.50	10	11	10	3	13.02

3. Results and discussions

a) Surface Current Density and Surface E-field Pattern

Fig. 5(a-c) shows the current densities on the antenna's radiating elements at 1.57 GHz, 2.10 GHz, and 2.4 GHz to demonstrate how the intended antenna functions. The current route is indicated by hedgehog signs, with the red color indicating the max density region and the blue color indicating a null density region of the surface current. At the three resonant modes of 1.57 GHz, 2.1 GHz, and 2.4 GHz, as shown in Fig. 5(a), the current intensity on the feed line as well as the slotted bottom edge of the ground on the left side of the ground plane is much greater than the current in other areas of the antenna. The feed line surface and the slotted bottom edge of the ground both contribute to the generation of the maximum current because the left-hand part of the ground is quarter-wave resonant and is being excited by the feed line. In this case, the length of the current route, or the resonant length, is

$$ln_{f_r} = \frac{\lambda}{4} \tag{1}$$

In this instance, λ stands for the wavelength of fundamental resonances in empty space. In patch antenna configuration, the ground layer acts as a radiator and generates extra reversed current. As illustrated in the Fig. 5(a), this reverse current has a significant influence on the lower frequency resonance mode at 2.57 GHz. At this resonance maximum current observed along feed line surface and slotted bottom edge of the ground. With increasing frequency, at second resonance 2.1 GHz, a large current move to the middle point i.e., intersection point of the vertical rectangular slots and horizontal rectangular slots on the patch radiator. Patch radiator-surface current has a significant influence on higher order resonance mode at 2.4 GHz. The highest density was seen in the slotted left section of the elliptical patch. For higher frequencies, there is a significant null density observed in the back radiator. The patch is a short length of low-impedance microstrip (almost half a wavelength) with an open circuit at each end. At each open circuit, the electric field is close to an anti-node, so it goes between high positive and high negative values. The magnetic field is very small because it is close to a node. Under the center of the patch, there is an electric field node and a magnetic field anti-node. This makes a line where the electric field

is zero and the magnetic field is high and low at different points. At each point on the lower surface, the magnetic field under the patch is equal to the amount of electric current on the surface. Most of the time, the radiation from the patch is thought of as coming from two magnetic dipoles, one at each end of the patch in the dielectric gap. The strength of the magnetic dipole field is given by the displacement current. The magnetic dipoles are in phase with each other and run the length of each slot. The sides of the patch don't spread out as much as the gaps at the ends. As with microstrip, most of the electric currents are on the bottom of the patch and on the ground plane right below it. The patch and ground currents are close to each other and go in different directions. The patch hides these currents, so they don't radiate. The surface E-field pattern at three resonances of the antenna without any slot in the patch and proposed antenna at 1.57 GHz, 2.1 GHz and 2.4 GHz is also included in Fig. 6(a-c). It can be seen that the magnitude of electric field intensity for the proposed antenna is less than the magnitude for the without slot antenna. Besides, in the E-field pattern, a bidirectional or Fig. 8 type shape is evident except at lower resonance 1.57 GHz. Here two circles touching at the center of Fig. 8 make up this pattern, which is quite popular. Consider a toroidal coil as an example, when the magnetic flux in the coil changes, the E field assumes the shape of Fig. 8 in an arbitrary plane cross-section that contains the toroid's central axis.

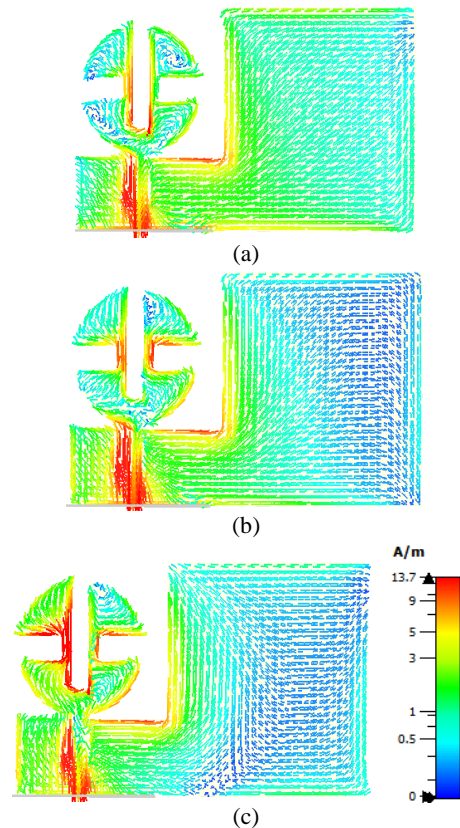


Fig. 5. Surface Current density at resonance point; (a) 1.57 GHz, (b) 2.1 GHz, (c) 2.4 GHz (color online)

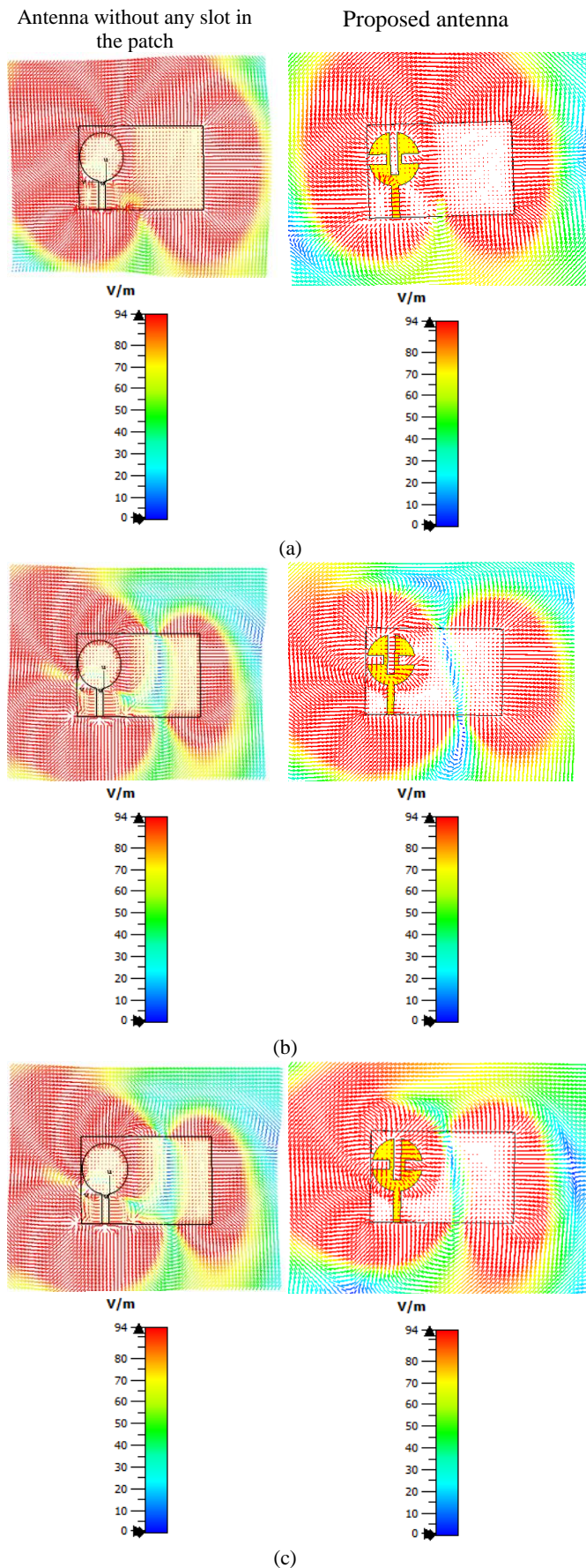


Fig. 6. The surface E-field propagation pattern without any slot in the patch and e proposed antenna at; (a) 1.57 GHz, (b) 2.1 GHz, (c) 2.4 GHz (color online)

b) Frequency Domain Experimental Results

Utilizing optimum parameter values the prototype is manufactured and shown in Fig. 7(a-b). The PNA network analyzer is used to determine the Reflection coefficient (dB) of the intended antenna. The PNA is capable of operating at frequencies ranging from 10 MHz to 67 GHz. Fig. 7(c) depicts the anechoic chamber where the antenna performance in terms of gain, radiation efficiency, and radiation pattern is experimentally assessed. The prototype manufactured has a -10 dB impedance bandwidth (IBW) from 1.3 GHz to 3.0 GHz and a minimal level of reflection coefficient less than -20 dB, as revealed in Fig. 8(a). The fractional bandwidth (FBW) reaches 79% for the experimental findings. The operating band has been shifted 100 MHz backward, which is insignificant. In the case of reflection coefficient, the prototype produces comparable results to the simulated results. The main reason why the simulated findings are different from the measured ones is because in the simulation we take into account the ideal qualities of the material. For instance, we can assume that the radiating element patch and ground are constructed from ideal electrical conductors. However, copper laid over Fr-4 substrate exhibits a degree of resistive behavior, leading to losses as well as reflections. This means that the measured result places a greater emphasis on reflection loss. Furthermore, variations in the proposed antenna's capacitive and inductive properties, brought on by manufacturing faults, contribute to the antenna's erroneous reflection coefficient. Although there is a discrepancy between both the simulation and the experimental result due to these causes, this is negligible for imaging applications which are not frequency resonance-dependent. Anechoic chambers, such as UKM's StarLab, are used to measure gain, radiation efficiency, and radiation characteristics. StarLab has a measuring capacity ranging from 650 MHz to 18 GHz. Fig. 8(b-c) show the measured highest gain over the frequency and radiation efficiency of the provided antenna. In the range 1.3 - 3.0 GHz, the fabricated antenna obtained an experimental peak gain of 4.9 dBi at 2.65 GHz, and the radiation efficiency is as high as 85%. There are relatively modest differences among experimental and simulated findings for gain and efficiency. This minor difference among the two outcomes is mostly due to manufacturing flaws. Adding a loss-free substrate with a higher cost to the presented antenna may enhance its gain and efficiency. Moreover, based on the measurement findings, it is possible to predict that the presented antenna with a superior manufacturing would solve this problem.

As illustrated in Fig. 9(a-b), the anticipated SEPDA radiation properties including co and cross polarization are investigated within the anechoic chamber. Fig. 9(a) depicts the radiation pattern in the xz plane ($\phi=0$), whereas Fig. 9(b) depicts the pattern in the yz plane ($\phi=90$) at lower resonance 1.57 GHz. Bi-directional radiation properties can be seen in the yz-plane. And almost omnidirectional radiation properties are reported in the xz-plane, by including a highest X-pol significantly lower than 10 dB for 1.57 GHz. In the yz-plane, at 1.57 GHz, the x-pol

element is relatively larger. Actually, the currents' vertical parts provide a major contribution to the antenna's radiation. The ground reverse extra currents, on the other hand, in addition to co-polarization in yz-plane does not make sense; rather, they strengthen the cross-polarization (x-pol) components [23, 24]. The fact that is also noticeable that experimental and simulated patterns are in reasonable agreement. Fig. 10(a) shows the 3D radiation pattern at 1.57 GHz, while Fig. 10(b) shows transparent view, revealing that it delivers outstanding omnidirectional characteristics.

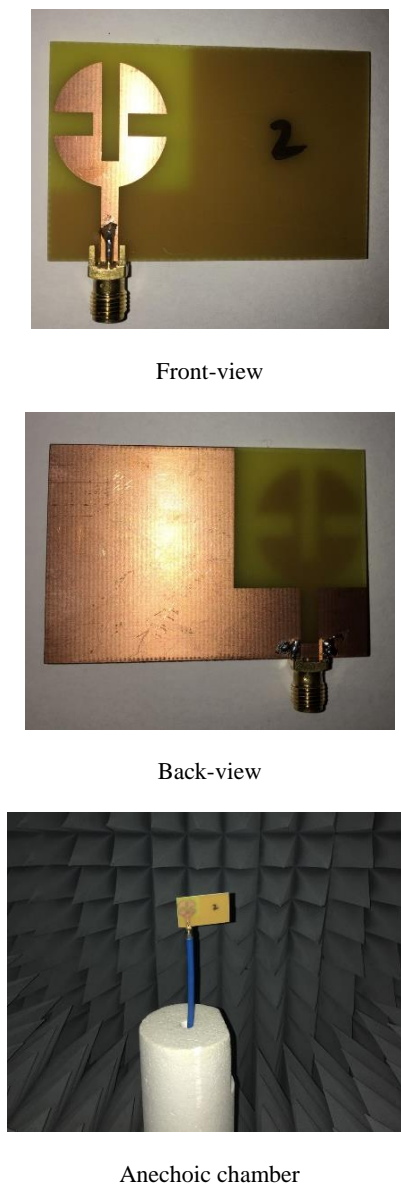


Fig. 7. Snapshot of the SEPDGA prototype and laboratory measurement setup

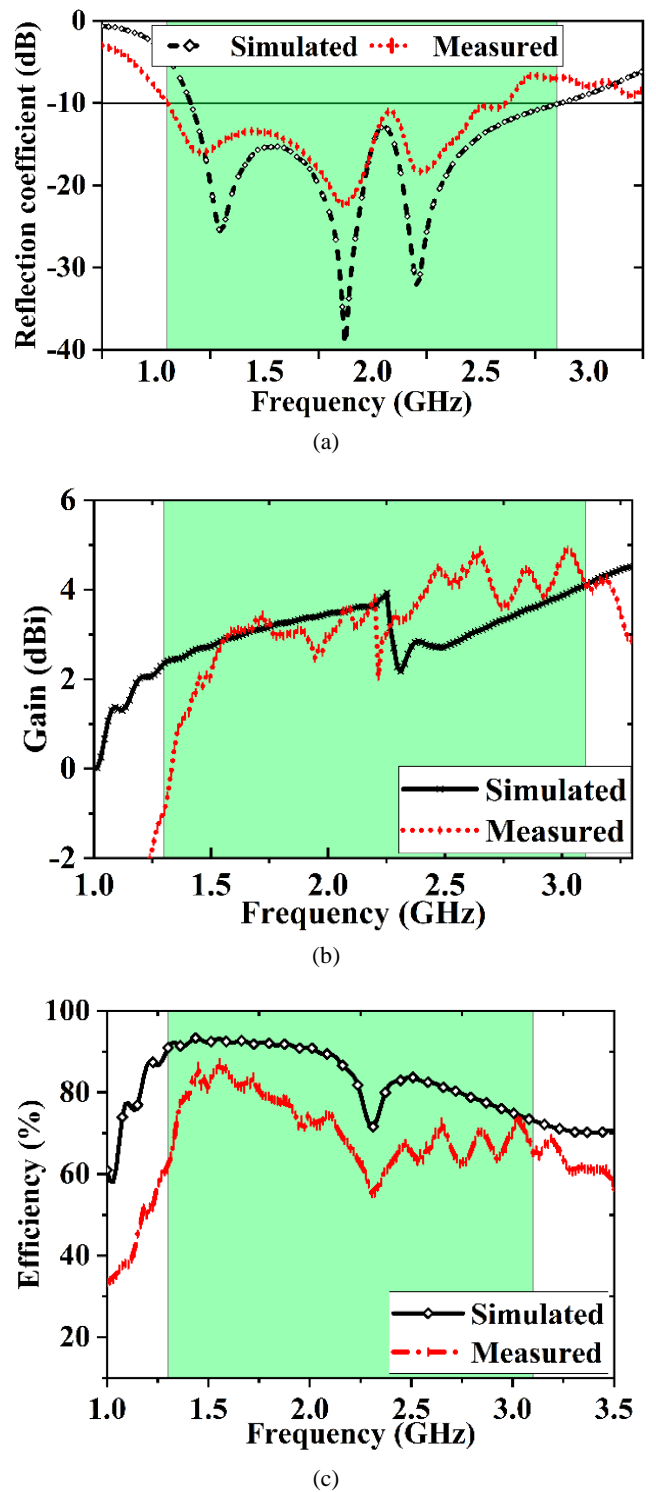


Fig. 8. Laboratory measurement outcomes; (a) Reflection coefficient (S_{11}), (b) Peak gain, (c) Radiation efficiency (color online)

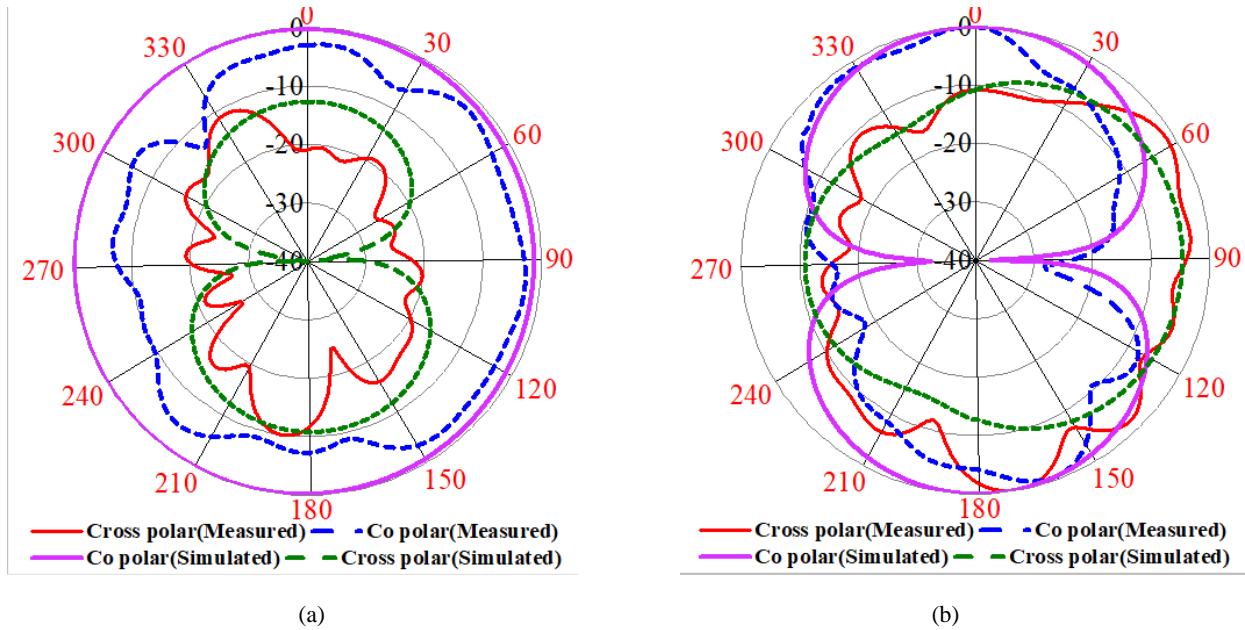


Fig. 9. Laboratory measurement radiation pattern outcomes at 1.57 GHz along; (a) xz-plane (phi=0), (b) yz-plane (phi=90) (color online)

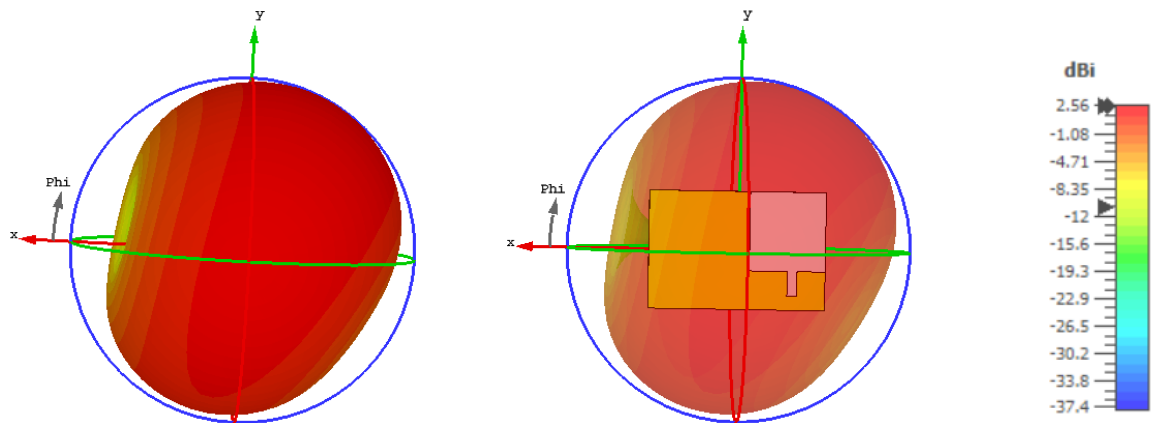


Fig. 10. 3-dimensional radiation pattern view at 1.57 GHz; (a) non-transparent view, (b) transparent view (color online)

c) Time-domain Analysis

As the antenna directly transmits short pulses, rather than continuous waves, the time-domain features of the wideband antenna are crucial. In order to achieve optimal wideband antenna performance, it must possess improved time-domain characteristics. The basic way for evaluating the pulse retention capability of the wideband antenna is to analyse its fidelity factor. The FF specifies the degree of similarity in between transmission and reception pulses. It also indicates the degree to which a pulse delivered by a wideband antenna is corrupted. For this investigation, two identical antennas, one acting as a transmitter (Tx) and the other as a receptor (Rx), are placed in 250 mm separation. The fidelity factor is related to the normalized transmitted and received pulses between Tx and Rx antennas. Normalized pulse magnitude between two antennas in face-to-face position are analyzed and included in Fig. 12. The

following formulas (2-3) can be used to study the normalized signals [25].

$$Rx'(t) = \frac{Rx(t)}{[\int_{-\infty}^{\infty} |Rx(t)|^2 dt]^{1/2}} \tag{2}$$

$$Tx'(t) = \frac{Tx(t)}{[\int_{-\infty}^{\infty} |Tx(t)|^2 dt]^{1/2}} \tag{3}$$

where, Rx(t) and Tx(t) represents the transmission and reception signal with respect to time. The FF is describing as follows (4):

$$FF = \max \int_{-\infty}^{\infty} Tx'(t)Rx'(t + \tau) dt \tag{4}$$

A fidelity factor (FF) value of 1 or 100% means that the received signal matches the input signal exactly, indicating that transmission did not cause any fluctuations or dispersion. In a face-to-face scenario, the proposed

antenna has a fidelity rating of 0.78, or 78 %. That indicates the antenna is capable of retaining 98% of the pulses. Moreover, it is evident from Fig. 12 that the signals received in face-to-face conditions are more comparable to those transmitted. Fig. 11(a-b) additionally depicts the E-field and H-field responses between the transmitter and receiving antennas in face-to-face scenario. The receiving antenna, as illustrated in figure, responds precisely with the emitting E-field and H-field. As a result, the highest density of e-field and H-field was observed along the Tx antenna and well recognized by the receiver.

Finally, as indicated in Table 2 the proposed antenna is compared to some related existing works on miniature wideband antennas for biomedical application. And for the comparative analysis dimension, substrate material, impedance BW, fractional BW, fidelity factor, peak gain over frequency, performance analyzation method and application are the criteria under consideration. It is apparent that the presented antenna offers a lightweight wideband antenna that might be used in microwave based biomedical applications.

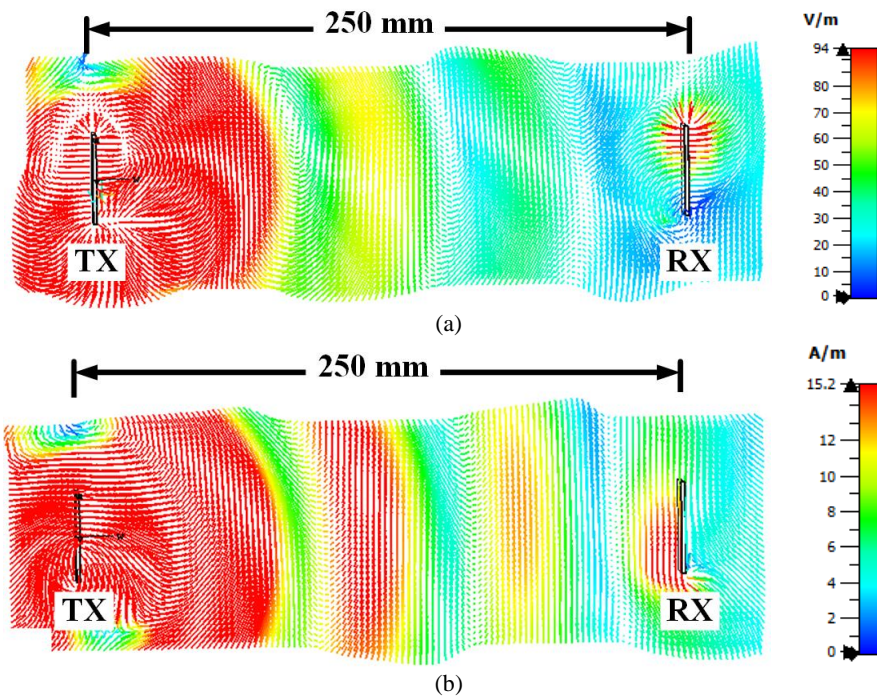


Fig. 11. Field response between transmitter and receiver; (a) E-field and (b) H-field (color online)

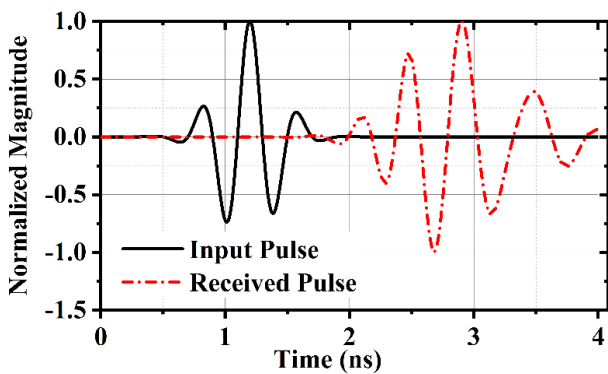


Fig. 12. Normalized magnitude of transmission and reception signal in face-to-face scenario (color online)

d) Imaging implementation

A biomedical imaging environment with antenna array configuration can be seen in Fig. 13(a-b), in which a phantom is covered by nine antenna components, each

covering a certain portion of the phantom. Approximately 20 mm separates the antenna from the skin layer, and 10 mm separates them from each other in such configuration. As an example of brain tumor detection, a synthetic tumor is implanted in CST simulation based Hugo's brain model which is displayed in Fig. 14. Nine antenna array is placed around the Hugo Model. Scattered parameters (S1,1, S2,1.....S7,1..S9,1) are then gathered for both tumor-bearing and tumor-free conditions and used in further calculations like image reconstruction. In Figs. 13(a) and 13(b), two cases exhibit a variation in scattering parameters due to malignancy, and that is a key feature for the detection of malignancy. The presence of malignancy changed the energy level; thus, the image can be constructed using this changed energy level. From the figure, we can notice that the S1,1; S6,1 and S7,1 parameter greatly fluctuated due to the presence of the tumor.

In addition, SAR (Specific absorption rate) assessment is required to preserve the safety control of MWI imaging devices and biocompatibility, since a brief level of radiation exposure could pose serious health risks.

The SAR performs an analysis of the absorption of electromagnetic radiation over the whole-body tissue when electromagnetic power is exposed. Every 1 g of tissue in the US is standardized at 1.6 w/kg, whereas every 10 grams in the EU is standardized at 2 w/kg [16]. This can

be shown in Fig. 14 where the highest SAR value for the Antenna is 0.608 W/kg for tissue averaged at 10 grams, which is substantially lower than the permissible level. It is thus reasonable to say that the antenna design presented has met all of the safety standards.

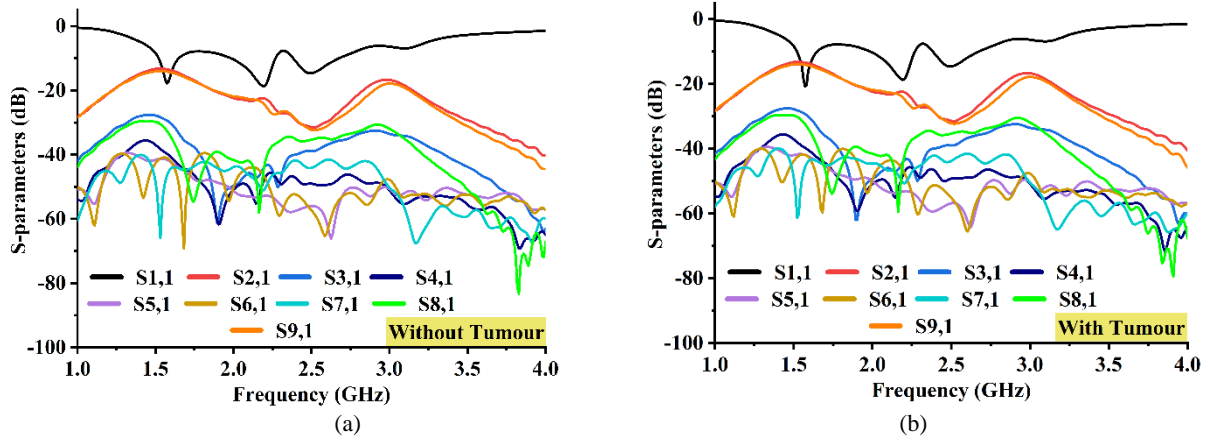


Fig. 13. Simulated scattering parameters; (a) with healthy head, (b) with tumor-bearing head (color online)

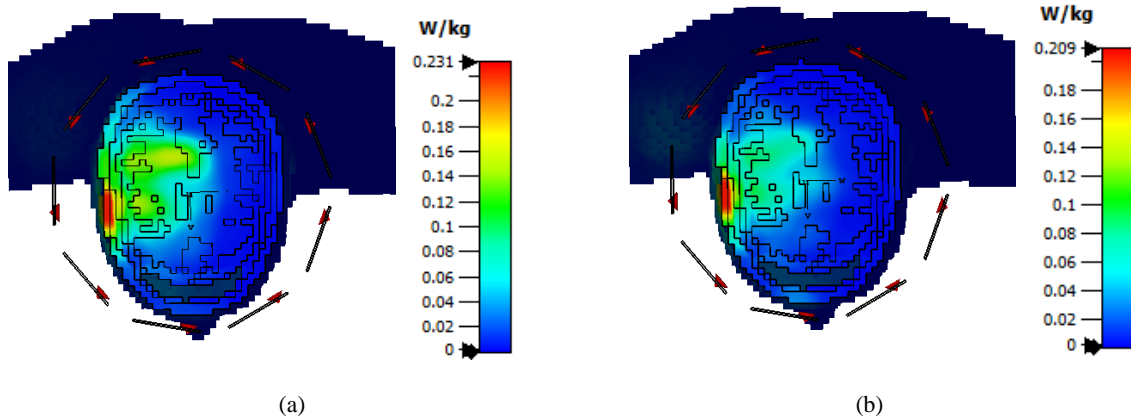


Fig. 14. Simulated Specific Absorption Rate (W/Kg) at; (a) 2.1 GHz, (b) 2.4 GHz (color online)

Table 2. A comparative analysis of the proposed SEPDKA performance with earlier reported works

Ref.	Dimension	Substrate	Substrate Layer	IBW (GHz)	FBW (%)	FF (%)	Gain (dBi)	Time/frequency domain	Application
[13]	50×60×1.5	Rogers RO4350B	1	2.06-2.61	23.55%	NR	2.45	Frequency domain	Head imaging
[26]	59×59×1.5	Rogers R04003C	2	0.9-1.3	36.36%	NR	3.10	Frequency domain	Head imaging
[15]	85×60×4.0	PDMS	5	1.16-1.94	53.8%	NR	NR	Frequency and Time domain	Head imaging
[27]	56×37×1.6	FR-4	1	1.45-2.52	53.90%	NR	2.4	Frequency domain	Head imaging
[28]	29.99×29.99×0.59	FR-4	1	0.6-1.3	73.68%	NR	<3	Frequency domain	Head imaging
[29]	50×44×1.52	Rogers RO4350B	1	1.70-3.71	74.3%	>95	>4	Frequency and Time domain	Head imaging
[30]	79×68.28 mm ²	FR-4	1	1-2	10%	NR	NR	Frequency domain	Head imaging
[Proposed]	37×56×1.5	FR-4	1	1.3-3.0	79%	78	≈ 4.9	Frequency and Time domain	Head imaging

NR= Not reported
λ =Lower most frequency wavelength

4. Conclusion

A novel planar antenna for biomedical applications in S-band frequencies is proposed that offers wide bandwidth, decent gain and improved efficiency. The overall dimensions were tuned to be $56 \times 37 \times 1.6 \text{ mm}^3$ and wavelength based to be $0.26 \times 0.17 \times 0.007 \lambda^3$ (λ is the lowest recorded frequency's wavelength). The layout of the SEPDGA has a broad bandwidth of 1.8 GHz and functions from 1.4 GHz to 3.2 GHz with a minimal reflection coefficient of -40 dB . A radiation efficiency of over 90 % was provided by the proposed design with a peak gain of over 4.5 dBi on the FR-4, a very cheap substrate. Laboratory measurements of the SEPDGA prototype demonstrate that it provides large bandwidth of 1.7 GHz with a minimal reflection coefficient of -20 dB and three resonance mode. The intended antenna features a stable-omnidirectional radiation properties, allowing this to be implanted on the targeted area in on both the front and back orientation. The designed antenna has a fidelity value of 0.78, which means it can preserve 78 % of the signal. Finally, the results of the total simulation and laboratory measurements show that the prototype in consideration is suited for biomedical head imaging applications.

Acknowledgement

This work is supported by the Patuakhali Science and Technology University Research Grant Code: PSTU/RTC-B/01/15/26(52).

References

- [1] R. Azim, R. Azim, A. M. H. Meaze, A. Affandi, M. M. Alam, R. Aktar, M. S. Mia, T. Alam, M. Samsuzzaman, M. T. Islam, *International Journal of Microwave and Wireless Technologies* **13**, 486 (2021).
- [2] M. A. Dorostkar, R. Azim, M. Islam, *Procedia Technology* **11**, 1285 (2013).
- [3] M. Alibakhshi-Kenari, M. Naser-Moghadasi, R. A. Sadeghzadeh, B. S. Virdee, E. Limiti, *Radio Science* **51**, 1109 (2016).
- [4] M. Alibakhshikenari, B. S. Virdee, E. Limiti, *Radio Science* **52**, 1510 (2017).
- [5] M. Gupta, V. Mathur, A. Kumar, V. Saxena, D. Bhatnagar, *Frequenz* **73**, 321 (2019).
- [6] S. Palanivel Rajan, C. Vivek, *Journal of Electrical Engineering & Technology* **14**, 923 (2019).
- [7] M. S. Islam, S. K. Azam, A. Z. Hossain, M. I. Ibrahimy, S. Motakabber, *Engineering Science and Technology, International Journal* **35**, 101112 (2022).
- [8] R. Azim, A. T. Mobashsher, M. T. Islam, N. Misran, *International Conference on Microwave and Millimeter Wave Technology* **2010**, 1987 (2010).
- [9] A. Mobashsher, K. Bialkowski, A. Abbosh, S. Crozier, *PLoS One* **11**, e0152351 (2016).
- [10] R. Inum, M. M. Rana, M. A. Quader, 3rd International Conference on Electrical Engineering and Information Communication Technology (ICEEICT) **2016**, 1 (2016).
- [11] L. Chen, C. Wang, H. Li, S. Lan, *International Symposium on Antennas and Propagation (ISAP)* **2017**, 1 (2017).
- [12] R. Scapaticci, J. Tobon, G. Bellizzi, F. Vipiana, L. Crocco, *IEEE Transactions on Antennas and Propagation* **66**, 7328 (2018).
- [13] A. Salleh, C. C. Yang, M. S. J. Singh, M. T. Islam, *Int. J. Eng. Technol.* **8**, 162 (2019).
- [14] A. S. Alqadami, N. Nguyen-Trong, B. Mohammed, A. E. Stancombe, M. T. Heitzmann, A. Abbosh, *IEEE Transactions on Antennas and Propagation* **68**, 183 (2019).
- [15] A. S. Alqadami, K. S. Bialkowski, A. T. Mobashsher, A. M. Abbosh, *IEEE Transactions on Biomedical Circuits and Systems* **13**, 124 (2018).
- [16] M. S. Talukder, M. M. Alam, M. T. Islam, M. Moniruzzaman, R. Azim, A. G. Alharbi, A. I. Khan, M. Moinuddin, M. Samsuzzaman, *Chinese Journal of Physics* **77**, 250 (2022).
- [17] M. M. Alam, M. S. Talukder, M. Samsuzzaman, A. I. Khan, N. Kasim, I. M. Mehedi, R. Azim *Chinese Journal of Physics* **77**, 233 (2022).
- [18] M. S. Talukder, M. Samsuzzaman, M. T. Islam, R. Azim, M. Z. Mahmud, M. T. Islam, *Chinese Journal of Physics* **72**, 310 (2021).
- [19] M. Rokunuzzaman, M. Samsuzzaman, M. T. Islam, *IEEE Antennas Wirel. Propag. Lett.* **16**, 169 (2016).
- [20] M. Z. Mahmud, M. T. Islam, N. Misran, S. Kibria, M. Samsuzzaman, *IEEE Access* **6**, 44763 (2018).
- [21] M. Samsuzzaman, M. T. Islam, M. T. Islam, A. A. Shovon, R. I. Faruque, N. Misran, *Microwave and Optical Technology Letters* **61**, 2110 (2019).
- [22] M. Rokunuzzaman, A. Ahmed, T. C. Baum, W. S. Rowe, *IEEE Transactions on Antennas and Propagation* **67**, 5093 (2019).
- [23] X. Qing, Z. Chen, *IET Microwaves, Antennas & Propagation* **3**, 889 (2009).
- [24] H.-D. Chen, *IEEE Transactions on Antennas and Propagation* **51**, 1982 (2003).
- [25] G. Quintero, J.-F. Zurcher, A. K. Skrivervik, *IEEE Transactions on Antennas and Propagation* **59**, 2502 (2011).
- [26] I. Merunka, A. Massa, D. Vrba, O. Fiser, M. Salucci, J. Vrba, *International Journal of Antennas and Propagation* **2019**, 1 (2019).
- [27] M. M. Hasan, M. Samsuzzaman, M. S. Talukder, M. T. Islam, R. Azim, M. A. Masud, 2nd International Conference on Sustainable Technologies for Industry 4.0 (STI), **2020**, 1 (2020).
- [28] M. S. B. Nesar, N. Chakma, M. A. Muktedir, A. Biswas, *International Conference on Innovations in Science, Engineering and Technology (ICISSET)* **2018**, 157 (2018).
- [29] A. Hossain, M. T. Islam, M. E. Chowdhury, M. Samsuzzaman, *IEEE Access* **8**, 185698 (2020).
- [30] B. Sohani, B. Khalesi, N. Ghavami, M. Ghavami, S. Dudley, A. Rahmani, G. Tiberi, *Biomedical Signal Processing and Control* **61**, 102001 (2020).

*Corresponding author: sobuz@pstu.ac.bd